Journal of Cleaner Production 235 (2019) 461–472

Contents lists available at ScienceDirect

Journal of Cleaner Production

journal homepage: www.elsevier.com/locate/jclepro

Characterization and performance of high volume recycled waste glass and ground granulated blast furnace slag or fly ash blended mortars

G. Liu*, M.V.A. Florea, H.J.H. Brouwers

Department of the Built Environment, Eindhoven University of Technology, P. O. Box 513, 5600MB, Eindhoven, the Netherlands

ARTICLE INFO

Article history:
Received 28 January 2019
Received in revised form
5 June 2019
Accepted 30 June 2019
Available online 2 July 2019

Handling Editor: Vladimir Strezov

Keywords:
High volume
Recycled waste glass
GGBS and fly ash
Synergistic effect
Microstructure
Rapid chloride migration

ABSTRACT

The application of recycled waste glass powder in high volume (60%) of ground granulated blast furnace slag (GGBS) or fly ash blended cement binder is shown in this study. The hydration kinetics, hydration products of different binder systems were studied by calorimetric and X-ray diffraction test. To investigate the microstructure properties of bended binders modified by glass powder, the mercury intrusion porosimetry test and scanning electron microscopy were conducted. The resistance to chloride penetration was evaluated by the rapid chloride migration test. The incorporation of recycled waste glass in slag or fly ash blended cement improves the reaction intensity while decreases the duration of induction period. The calcium hydroxide content of blended samples (91 days) was decreased after the incorporation of waste glass powder, while a densification effect on the capillary pores (10–100 nm) and lowers the total porosity of waste glass containing ternary binders were observed. From the SEM analysis, a dense microstructure and inter transition zone can be found in recycled waste glass blended samples. The waste glass powder modified slag or fly ash blended mortars exhibit a significant enhancement of resistance to chloride migration. Furthermore, a synergistic effect on the mechanical performance of large volume GGBS blended mortars containing recycled waste glass was identified, which presented the highest compressive strength among all waste blended samples.

1. Introduction

As the most used building material, more than 20 billion tons of concrete are produced every year worldwide. To meet the demand of worldwide construction, every year, large amounts of natural resource are consumed for cement manufacturing. About 1.5 tonnes of raw materials are consumed for each tonne of cement production; in addition, 120–160 kWh of energy is necessary (Feiz et al., 2015). The high energy and natural resources consumption involved with cement manufacture, induces a serious environmental impact. As a consequence, the application of alternative supplementary cementitious materials (SCMs), for example, GGBS, fly ash and silica fume (Yang et al., 2015), even recycled waste glass (Torres-Carrasco and Puertas, 2015) to partially replace OPC in concrete, attracted more and more attention.

The application of GGBS and fly ash as SCMs in concrete attracted more focus for the purpose of CO_2 reduction and sustainable application of industrial by-products in the past decades (Crossin, 2015). Generally, a low replacement ratio of cement by GGBS or fly ash can significantly enhance the compressive strength compared to plain cement. In addition, the microstructural densification of blended concrete is observed due to the products of pozzolanic reaction, and as a consequence, low permeability can be induced (Häkkinen, 1993; Leng et al., 2000a). Regarding hydraulic and pozzolanic activity of GGBS in concrete (Bijen, 1996; Bouikni et al., 2009; Chen and Brouwers, 2007), many studies presented a various replacement ratio of GGBS in concrete production from a low level (10%–30%) to high level (50%–80%) with a less strength reduction in early age (Mo et al., 2015). Compared to GGBS, fly ash exhibits a lower reactivity in concrete. The high volume fly ash blended cement usually shows a lower mechanical performance at the early age (Kurda et al., 2018)(Rashad, 2015) and a poorer performance of resistance for chloride migration than that of the low replacement level sample (Ranjbar et al., 2016). In some studies, combining the use of fly ash and GGBS presents a superior mechanical performance and durability than applying these materials alone (Gholampour and Ozbakkaloglu, 2017; Rashad, 2015). However, in some cases with high replacement ratio, the total pore volume was increased compared to plain cement samples, and as a

* Corresponding author.
E-mail address: G.Liu@tue.nl (G. Liu).

https://doi.org/10.1016/j.jclepro.2019.06.334
0959-6526/

consequence, a decrease of compressive strength was observed (Kayali and Sharfuddin Ahmed, 2013; Zeng et al., 2012).

In recent years, recycled waste glass (a non-degradable solid material, mostly soda-lime glass) has attracted more attention in the sustainable application in construction materials. Some waste glass fractions cannot be recycled to manufacture the new glass products because it is too fine to meet the manufacturing specification, while increasing the pressure of landfill. At the same time, fine waste glass powder can exhibits a significant pozzolanic reactivity, which is due to the high amorphous silica content and was reported to be used as SCMs in concrete (Liu et al., 2018; Shao et al., 2000). An enhanced mechanical performance and dense microstructure of concrete by incorporating a low content of waste glass particles was proved (Yazıcı, 2007). In addition, The fine glass particles exhibited a higher pozzolanic activity than that of fly ash (Schwarz and Neithalath, 2008). However, the high volume addition of waste glass in cementitious system still shows a poor mechanical performance of concrete even it can reach a comparable strength as OPC after 1 year (Du and Tan, 2017). Unlike GGBS and fly ash, there is a limited research related to the large volume of waste glass as a binder in concrete (Du and Tan, 2014; Liu et al., 2019). However, in previous studies, recycled waste glass was indicated to show an enhancement of resistance to water and chloride penetration (Lee et al., 2018).

Combining the use of different SCMs in concrete can induce a synergic effect, which contributes to a better mechanical performance or durability than using it only (Keulen et al., 2018; Van Tuan et al., 2011; Wan et al., 2018). However, the report of combining waste glass powder with slag or fly ash is rare. The waste glass addition can improve the mechanical performance of high volume fly ash blended concrete (Siad et al., 2018). In addition, an improvement of the mechnical property of GGBS concrete containing recycled waste glass powder also was reported (Ramakrishnan et al., 2017). These limited studies indicate that the combined application of recycled waste glass with other SCMs is beneficial for the concrete performance. However, the modification mechanism and durability performance of waste glass powder blended ternary cement binders are still not clear. To optimize the performance of sustainable concrete containing recycled waste glass, GGBS and fly ash as binders, many related aspects, such as hydration kinetics, durability performance, and microstructure characterization need further study.

The present study includes a comparative evaluation of the mechanical performance, resistance for rapid chloride migration and microstructure between different binary mortars containing recycled waste glass, GGBS or fly ash. In addition, the effects of recycled waste glass combination on the reaction kinetics, durability, strength and porosity structure of OPC-GGBS-recycled waste glass and OPC-fly ash-recycled waste glass ternary binder system are studied. The aim is to optimize the large volume application by combining recycled waste glass with GGBS and fly ash in concrete.

2. Materials and methods

2.1. Materials

The cement in this study was CEM I 52.5 R which produced by ENCI, Netherlands. The recycled waste glass powder, ground granulated furnace slag (GGBS), and fly ash were selected as the SCMs in this study. The recycled mixed color glass fractions supplied by a glass recycling plant were grounded into powder by ball milling. Ground granulated blast furnace slag (GGBS) was provided by ENCI, IJmuiden, Netherlands. The fly ash was provided by Vliegasunie B.V., the Netherlands. The chemical composition of raw materials are shown in Table 1 and the mineral composition of materials are exhibited in Fig. 1. The d_{50} particle size of cement, waste glass powder, GGBS, and fly ash were 8.08 μm, 10.97 μm, 19.38 μm and 23.27 μm respectively. The particle size distribution of raw materials are shown in Fig. 2.

2.2. Methods

2.2.1. Mortars preparation

The mixtures design of mortars is shown in Table 2. The different binders were mixed with water and sand by a Hobart mixer. Then the fresh mortars were filled into the plastic mould of 40 mm × 40 mm × 160 mm and vibrated for 60 s and covered with the plastic film for 24 h. After that, the prisms were demould and covered by plastic film for ambient curing until further testing.

2.2.2. Raw material characterization

X-ray diffraction (Bruker D2 PHASER) with Co tube was used to study the reaction products of raw materials and different blended mixtures cured after 91 days. The crushed pastes samples were immersed in acetone to cease hydration. Then, a ball mill was used to mill the crushed samples into powder for XRD.

Table 1
Chemical composition and physical properties of cement, waste glass, GGBS and fly ash.

Chemical composition	CEM I 52.5 R (%)	Waste glass (%)	GGBS (%)	Fly ash (%)
Na_2O	/	14.651	/	/
MgO	1.712	1.298	8.57	1.141
Al_2O_3	3.793	1.93	13.214	26.98
SiO_2	16.188	68.328	29.407	51.442
SO_3	4.055	0.086	2.639	1.121
K_2O	0.187	0.702	0.424	1.84
CaO	67.968	11.904	42.665	5.83
TiO_2	0.277	0.062	1.487	1.78
Cr_2O_3	0.01	0.117	0.001	0.034
MnO	0.094	0.022	0.398	0.057
Fe_2O_3	3.589	0.364	0.366	8.271
ZnO	0.1	0.009	/	0.022
BaO	0.005	0.061	0.081	/
PbO	0.005	0.05	/	0.009
P_2O_5	0.42	/	/	0.849
Cl	0.041	0.019	0.011	/
LOI	0.72	1.34	1.15	2.27
Specific density (g/cm^3)	3.10	2.51	2.93	2.30
Specific surface area (m^2/g)	1.0039	0.9918	0.3649	0.8145

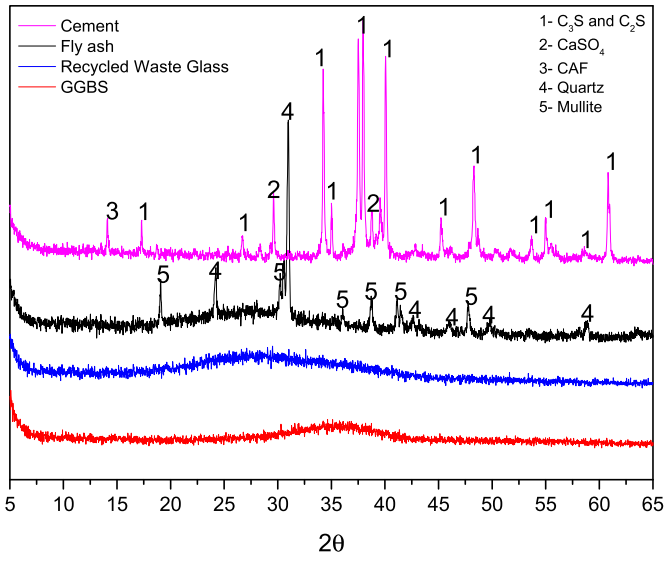

Fig. 1. XRD patterns of materials.

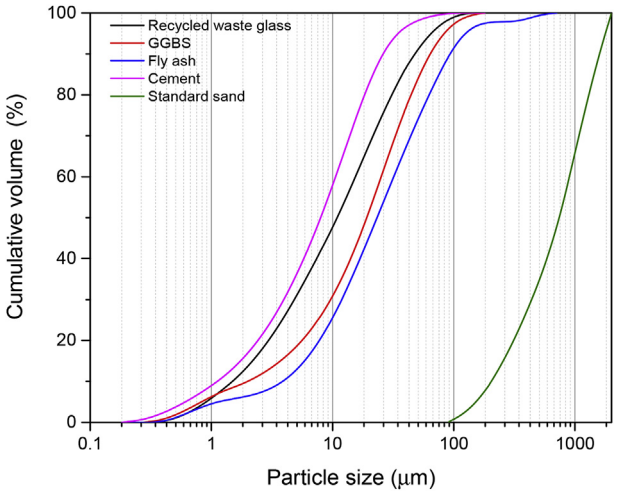

Fig. 2. PSD of applied materials.

The XRF tests were conducted by using an X-ray fluorescence spectrometer (PANalytical Epsilon 3). The pressed powder sample was prepared and for the element analysis.

The particle size distributions of raw materials were tested by laser granulometry (Master sizer 2000).

2.2.3. Slump flow and apparent density of mortars

The slump-flow of fresh mortars was conducted by the flow table test, according to EN 1015–3. An average value of two tested diameters were recorded by using a standard conical ring.

The apparent density of mortars were determined by mass and volume of mortar samples after demoulding.

2.2.4. Isothermal calorimetry

The reaction heat development was conducted by using an isothermal calorimeter (TAM Air, Thermometric). The test duration was set to 125 h at a temperature of 20 °C. The data of heat development was calculated by mass of total powder.

2.2.5. Thermogravimetric test

The calcium hydroxide content of mixtures were calculated by the results of thermal-gravimetric (TG) analysis, which was conducted in a STA 449 F1 instrument. The temperature range was set from 40 °C to 1000 °C, the heat rate was 10 °C/minute and the protection gas was N_2.

2.2.6. Rapid chloride migration test

Cylindrical cores with a diameter of 100 mm were cut from the cubes after 91 days curing. Then the cylindrical cores were sliced into specimens with 50 mm height for the RCM test. Before the test, each sample was vacuumed and saturated with lime water. The vacuum-saturation was conducted as following processes: specimens were placed in a desiccator connected to a vacuum pump, then pressure was kept constant at 40 mbar for 3 h. After that the lime water was filled in the desiccator slowly until the specimens were immersed completely. After this, the vacuum was maintained for one more hour, then turn off the vacuum pump and kept the drilled cores in solution for 18 h. The equipment for RCM test is shown as Fig. 3. The 0.3 M NaOH solution and the 10% (wt.) NaCl solution were prepared.The voltage of the test used in this study was selected as the Table 3 (Spiesz and Brouwers, 2012). The D_{RCM} coefficient was calculated by the equation (1):

$$D_{RCM} = \frac{RTL}{zF(U-2)} \times \frac{x_d - \alpha\sqrt{x_d}}{t_{RCM}} \quad (1)$$

$$\alpha = 2\sqrt{\frac{RTL}{zF(U-2)}} \times erf^{-1}\left(1 - \frac{2c_d}{c_0}\right) \quad (2)$$

R-universal gas constant (8.314 $Jmol^{-1}K^{-1}$), T-temperature (293 K), L-thickness of the sample (0.05 m), U -applied external voltage (V), z - ion valance, F-Faraday constant (96.485 C/mol), x_d-average chloride penetration depth, α-laboratory constant, t_{RCM}-duration of the test, erf^{-1}-inverse of error function, c_d-chloride concentration at which the colour changes (0.07 N), c_0-chloride concentration in the catholyte solution (2 N).

Table 2
Mixture design of mortars.

Sample ID	Cement (wt. %)	Fly ash (wt. %)	GGBS (wt. %)	Glass powder (wt. %)	w/b	Sand/binder	
OPC	100	0	0	0	0.5	2.5	Reference
G60	40	0	0	60	0.5	2.5	Binary binder sample
S60	40	0	60	0	0.5	2.5	
F60	40	60	0	0	0.5	2.5	
S10G50	40	0	10	50	0.5	2.5	Ternary binder sample
S30G30	40	0	30	30	0.5	2.5	
S50G10	40	0	50	10	0.5	2.5	
F10G50	40	10	0	50	0.5	2.5	
F30G30	40	30	0	30	0.5	2.5	
F50G10	40	50	0	10	0.5	2.5	

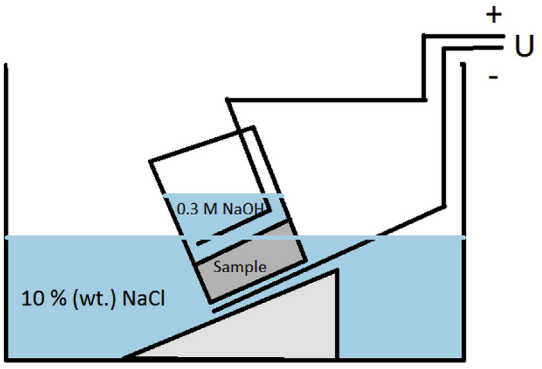

Fig. 3. Sketchy representation of RCM test (Spiesz and Brouwers, 2012).

Table 3
Selection of duration and voltage of the rapid chloride migration test.

I_{30} (mA)	U (V)	T (h)
<5	60	96
$5 \leq I_{30} \leq 10$	60	48
$10 \leq I_{30} \leq 15$	60	24
$15 \leq I_{30} \leq 20$	50	24
$20 \leq I_{30} \leq 30$	40	24
$30 \leq I_{30} \leq 40$	35	24
$40 \leq I_{30} \leq 60$	30	24
$60 \leq I_{30} \leq 90$	25	24
$90 \leq I_{30} \leq 120$	20	24
$120 \leq I_{30} \leq 180$	15	24
$180 \leq I_{30} \leq 360$	10	24
≥ 360	10	6

2.2.7. Mercury intrusion porosimetry

The mercury intrusion porosimetry (Micromeritics) was conducted to study the pore size distribution of mortars. The mortars after 90 days curing were crushed into small fractions (2 mm–4 mm) for analysis. The intrusion pressure is from 0 to 227 MPa.

2.2.8. Scanning electron microscopy

The microstructure of crushed mortar samples was tested by Scanning Electron Microscopy (Phenom Pro). Different mortar samples were immersed in isopropanol to cease the hydration, then samples were dried at 40 °C. After that dried mortar samples were embedded by resin and polished. Before the observation by Phenom Pro, all samples were coated by Au.

2.2.9. Strength test

The strength tests were conducted according to EN 196–1. Mortars (40 mm × 40 mm × 160 mm) were casted and. The tested ages were 7, 28, 56 and 91 days. The flexural strength was tested with prism samples, and an average of three results was recorded. After the flexural strength test, samples were used to test compressive strength. An average of six results was recorded as the compressive strength.

3. Results and discussion

3.1. Fresh properties and density of mortars

The slump-flow results of fresh blended mortars are shown in Fig. 4. It is observed that the fresh plain sample (OPC) presents a slump flow of 20 cm; when 60% cement was replaced by fly ash, slag, or waste glass powder, the slump flow was 23.25 cm, 21.85 cm, and 20 cm, respectively. Samples containing a combination of recycled waste glass powder and fly ash show a decreasing slump flow with the increase of the glass powder proportion, as well as the samples containing the combination of recycled waste glass powder and GGBS. The high surface area and fine particle size of waste glass powder (as shown in Table 1 and Fig. 2) induced a higher water absorption compared to fly ash and GGBS, and as a consequence, a low flow ability was observed.

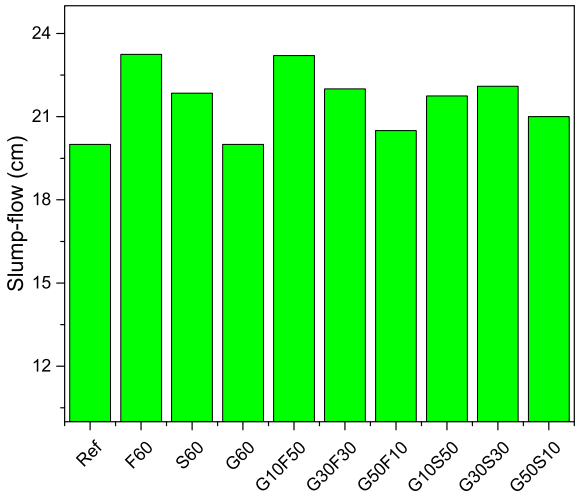

Fig. 4. Flow ability of fresh mortars.

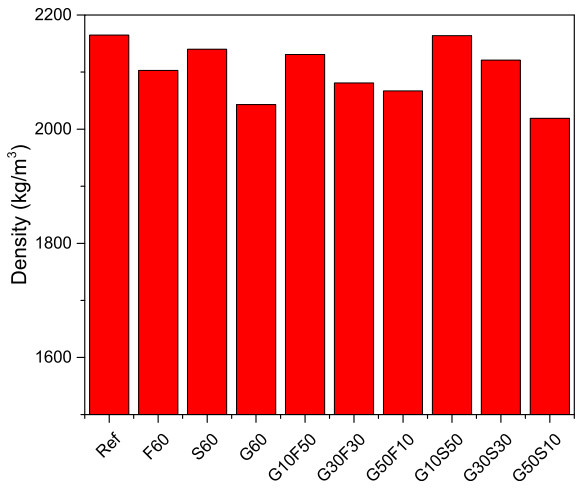

Fig. 5. Density of mortars.

It can be seen from Fig. 5 that the mortar containing 60% slag (S60) shows the highest density, while the sample incorporating fly ash (F60) presents higher density than the waste glass powder sample (G60). Fly ash exhibits a lower specific density and specific surface area than the recycled waste glass powder. However, due to its spherical shape, fly ash contributes to a better compactibility and therefore particle packing, finally, increasing the density of the mortar. For the waste glass containing GGBS or fly ash blended samples, the increase of waste glass amount results in a lower density; however, 10% of waste glass powder containing ternary mortars shows an enhancement on the density of samples compared to using fly ash and slag only. This indicates that 10% of recycled waste glass powder results in an improvement on packing of mortars containing GGBS or fly ash.

3.2. Hydration behaviour and production

3.2.1. Hydration behaviour

The reaction heat development of various pastes during the early hydration period are shown in Fig. 6. It can be seen in Fig. 6 (a) that all binary binders (G60, S60 and F60) show two main peaks of heat flow, and the intensity of these peaks are relatively low compared to the OPC sample.

The 60% of recycled waste glass powder binder (G60) takes a shorter duration to reach the first heat flow peak by 0.7 h, and the high volume fly ash prolongs the duration of induction period in comparison with OPC. It is reported that the fly ash can remove the calcium ions from the pore solution, so, the concentration of calcium becomes lower in the first hours, and the formation of calcium hydroxide and C–S–H is delayed, therefore the hydration is retarded (Jun-yuan et al., 1984; Ogawa et al., 1980; Plowman and Cabrera, 1984). Generally, the first heat flow peak of blended cement is induced by the reaction of C_3S and the following shoulder relates to the transfer of AFt to AFm (Mostafa and Brown, 2005). Apparently, the G60 exhibits a higher reactive intensity, featuring higher and earlier peaks compared to high volume GGBS and fly ash binary samples. Fine glass particles have been observed providing the additional Si and sodium source due to the amorphous structure of silica (Shi et al., 2005). As a consequence, a shorter induction period and higher reaction intensity in large volume waste glass powder binder (G60) can be observed by the increasing alkali and silica in pore solution (Nocuò-Wczelik, 1999).

In the heat flow result of OPC-fly ash-waste glass ternary samples, the heat generation of different samples is controlled by the different fly ash/waste glass proportion as shown in Fig. 6 (b). With the increase of the waste glass/fly ash ratio, the reaction rate and intensity are all enhanced. The lower waste glass/fly ash ratio is related to the longer induction period. The increasing proportion of waste glass powder decreases the retardation effect caused by fly ash. This improvement is probably induced by the acceleration effect of glass powder as shown above and the reduction of fly ash content.

The heat flow of OPC-GGBS-waste glass ternary binders are shown in Fig. 6 (c). The incorporation of glass powder reduces the time to reach the first heat flow peak. The increase of glass powder/GGBS proportion increases the reaction rate and intensity slightly.

3.2.2. Hydration products characterization

The hydration products of mixtures identified by XRD after 91 days are exhibited in Fig. 7 (a)-(c). The various peaks intensity and species are presented by samples with different proportions of waste glass powder, GGBS and fly ash.

When waste glass, GGBS and fly ash are used individually as 60% cement replacement in samples, all binary mixtures show weak peaks of calcium hydroxide compared to the reference sample (OPC). Among the blended samples, G60 exhibits the lowest peaks of calcium hydroxide. Meanwhile, a significant and wide peak can be found around 34°, which is induced by the poorly ordered C–S–H (Garbev et al., 2008a). The S60, F60, and OPC all present distinguishable peaks of ettringite, contrary to G60. In addition, the peaks of hydrotalcite are observed just in F60 and S60, which is a typical product during the reaction of GGBS and fly ash under alkali activation (Oh et al., 2010; Puertas and Fernández-Jiménez, 2003; Song and Jennings, 1999).

After the waste glass powder was incorporated with GGBS or fly ash, the peaks correspond to C–S–H are wider and more intense with higher waste glass powder amount in ternary systems; moreover, the intensity of calcium hydroxide peaks decrease significantly. The GGBS and fly ash ternary binders containing recycled waste glass powder show a significant influence on the

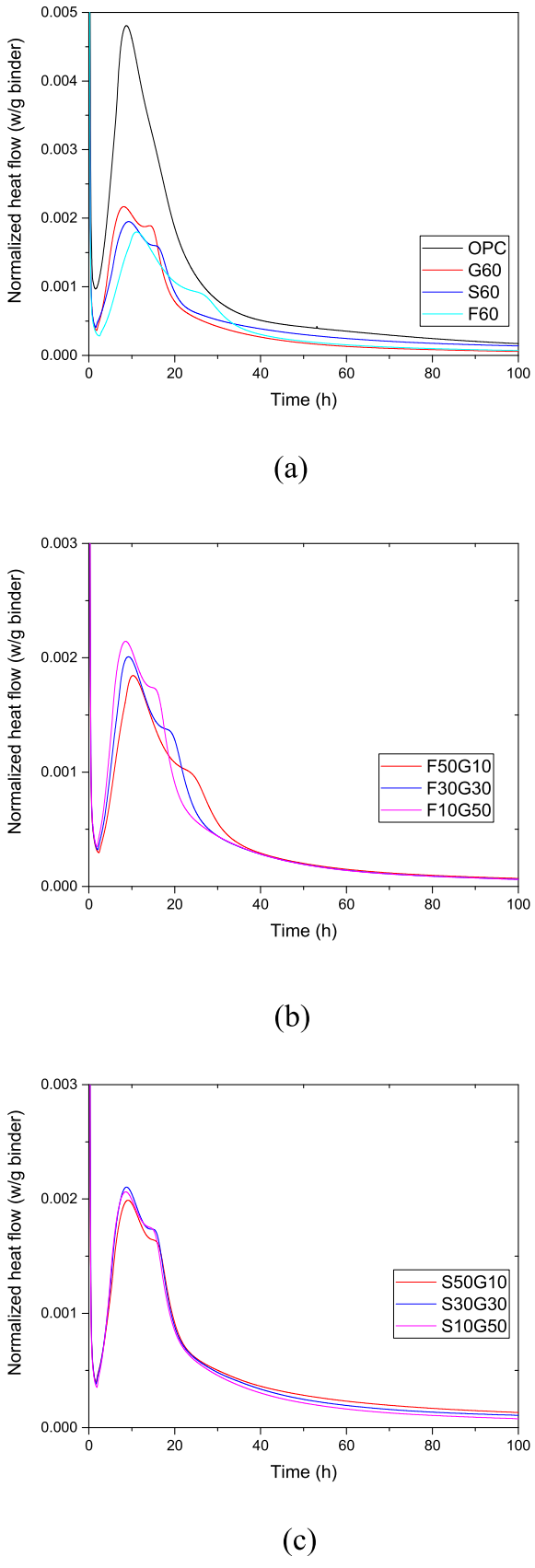

Fig. 6. Heat rate development of different mixtures (a) binary binders, (b) OPC-waste glass-fly ash ternary binders and (c) OPC-waste glass-GGBS ternary binders.

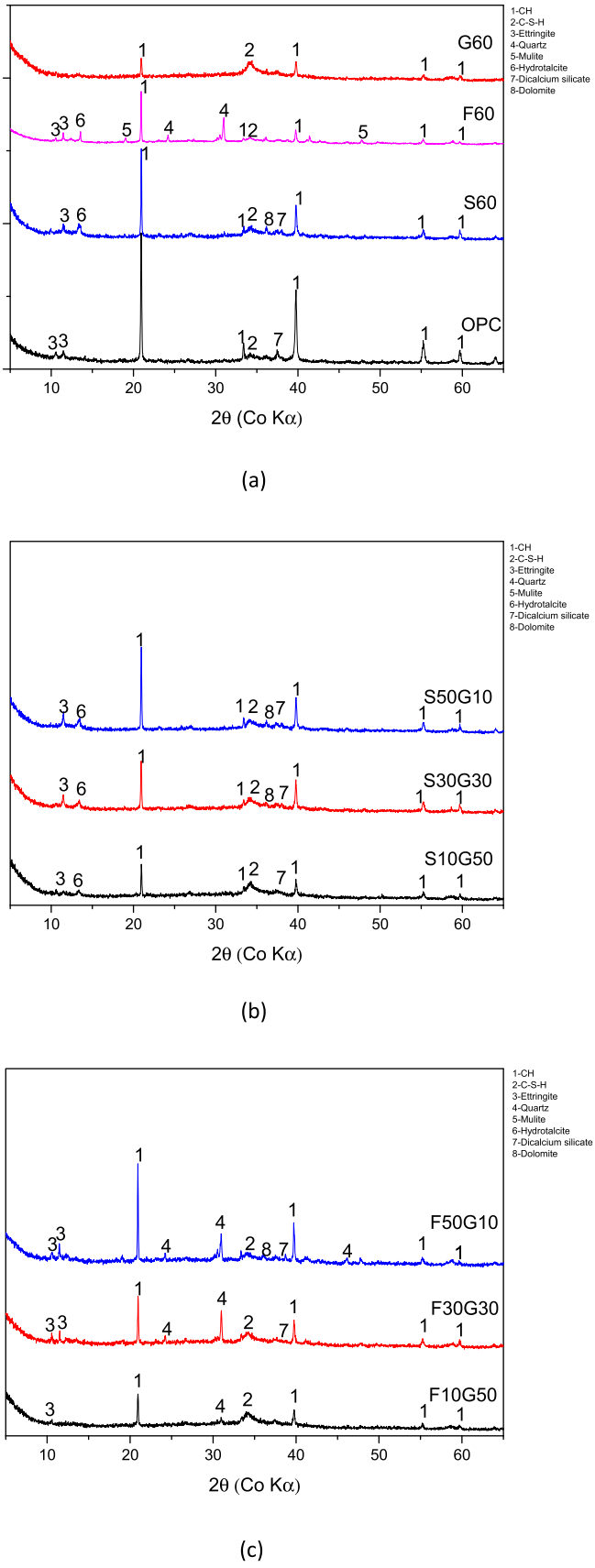

Fig. 7. XRD patterns of samples after 91 days curing (a) OPC and binary samples (b) cement-recycled waste glass-GGBS samples (c) cement-recycled waste glass-fly ash samples.

residual calcium hydroxide of mixtures after 91 days. As the results illustrate in Fig. 8, 60% recycled waste glass powder sample (G60) exhibits the lowest CH content compared to high volume of GGBS (S60) or fly ash samples (F60). Compared to the CH in mixtures after 7 days curing, the higher proportion of recycled waste glass powder in binders is related to more CH reduction. It can be seen that the higher waste glass powder proportion enhances the consumption of CH from cement hydration, which is due to the pozzolanic reaction of SiO_2 from the glass particles. Meanwhile, the increase of SiO_2 content in samples results in a lower Ca/Si ratio, leading to a poorly crystallized C–S–H (Garbev et al., 2008a, 2008b; Kumar et al., 2017), which shows a wild hump peak in X-ray diffraction.

3.3. Microstructure characterization

3.3.1. Pore structure

Fig. 9 (a) shows the cumulative pore volume of mortars containing 60% waste glass powder (G60), fly ash (F60) and slag (S60) compared with the plain cement sample (OPC). All curves show similar trend that pore volume keeps slow increasing in the range of more than 1000 nm. After that, a rapid increase in pore volume can be observed. High volume fly ash mortar shows the highest total pore volume compared with other samples. This is due to the slow pozzolanic reaction of fly ash particles (Yu and Ye, 2013; Zeng et al., 2012). Also the high volume of GGBS sample presents a higher porosity than the OPC, which can also be found in related studies (Li et al., 2014, 2010; Moon et al., 2006). On the contrary, the mortar (G60) shows a reduction of its total pore volume compared to the OPC sample, which indicates 60% of recycled waste glass powder results in no negative effect on the pore volume of mortar.

The cumulative pore volume of combining waste glass powder with fly ash or GGBS are shown in Fig. 9 (b) and Fig. 9 (c). It is interesting to notice the higher amount of recycled waste glass powder in ternary binders enhances pore volume of cement-GGBS-recycled waste glass powder mortars, but decreases the total pore volume of cement-fly ash-recycled waste glass powder samples. However, all ternary binder mortars still show a lower pore volume compared to the sample containing high volume GGBS or fly ash alone. This indicates a synergistic effects on total pore volume reduction was induced by the incorporation of waste glass powder with GGBS or fly ash.

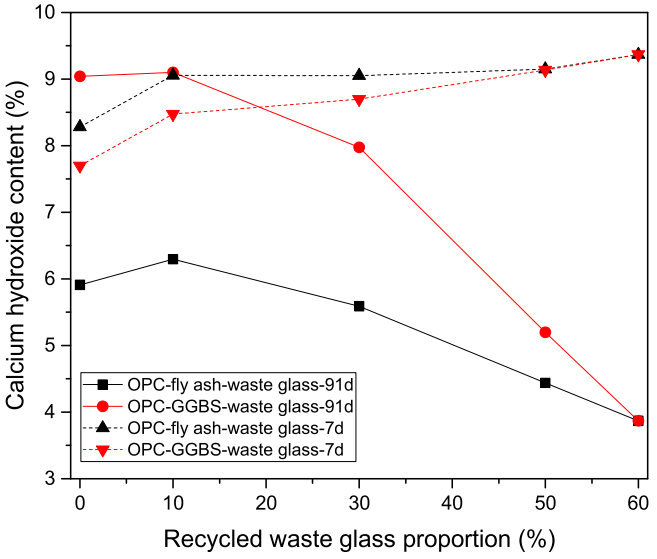

Fig. 8. Calcium hydroxide content of different mixtures after 7 days and 91 days.

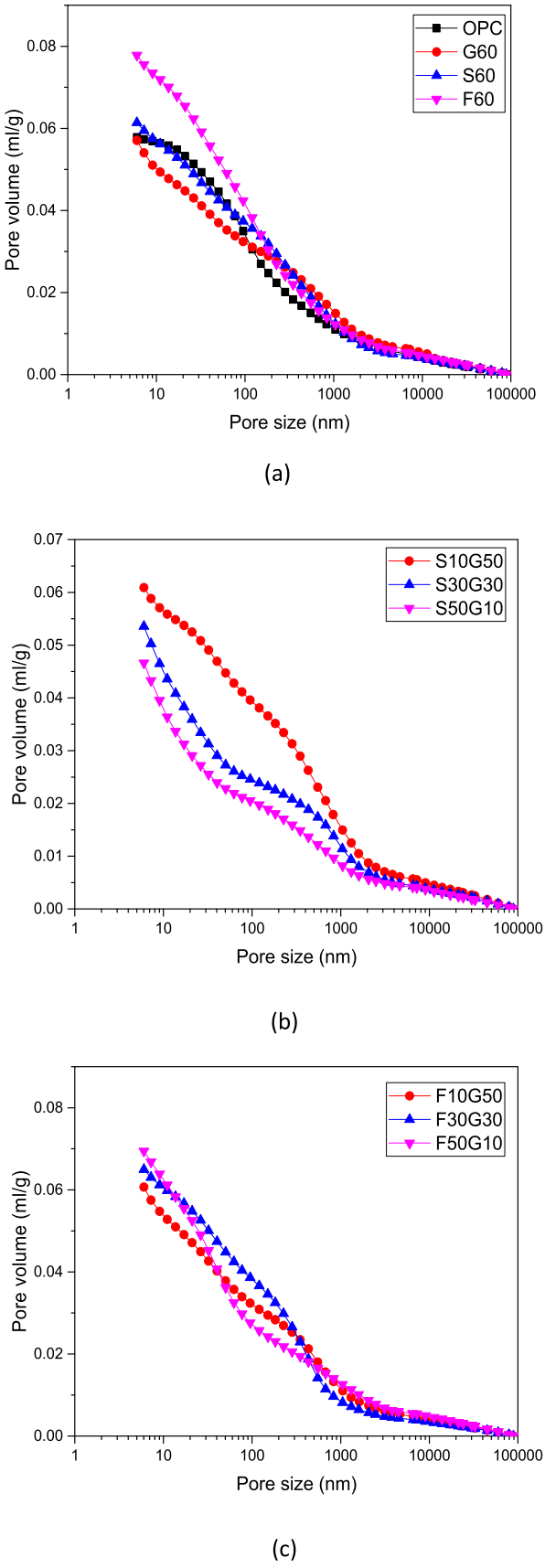

Fig. 9. Total pore volume results (a) OPC and binary samples (b) OPC-GGBS-waste glass samples (c) OPC-fly ash-waste glass samples.

Generally, a limited addition of GGBS and fly ash is helpful to the reduction of the concrete porosity (Leng et al., 2000a; Zuquan et al., 2007). However, the high volume SCMs in concrete results in higher total porosity and a limited improvement of durability (Zeng et al., 2012), and even the deterioration of mechanical performance of concrete (Kim and Lee, 2013). In the present study, 60% fly ash and 60% GGBS binary samples show higher porosity than the OPC, which also agrees with other studies (Gholampour and Ozbakkaloglu, 2017). Nevertheless, when the recycled waste glass is incorporated, some samples exhibit a reduction of porosity compared to OPC, for example, all cement-GGBS-recycled waste glass binder specimens and F10G50. This indicates that recycled waste glass powder not only exhibits less deterioration in total porosity but also shows a synergistic effect with GGBS and fly ash on the improvement microstructure of concrete. The porosity reduction of blended concrete can be induced by several effects, among which the pore refinement by the C–S–H of pozzolanic reaction by mineral addition. The products from the pozzolanic reaction gradually fills the volume of voids and contributes to the concrete strength. Another is the micro filler-effect: when the CH from cement hydration is insufficient for the reaction of the large volume pozzolanic materials, some unreacted particles can be the micro-filler in voids. These particles block the connection between pores and induce the effect on water penetration and ion transportation (Wongkeo et al., 2014). Furthermore, since the pozzolanic materials show different particle size and morphology, a specific mix design can introduce a dense packing for concrete, which presents a denser microstructure and a better mechanical performance (Brouwers, 2016).

The pore size distribution of mortars containing 60% recycled waste glass powder (G60), GGBS (S60), fly ash (F60) and the plain sample (OPC) are shown in Fig. 10 (a). It can be seen that the OPC shows a main peak and continuous pore distribution, and F60 exhibits a similar shape of pore size distribution as OPC, but a higher volume of pores less than 10 nm, and a small second peak between 10 nm–100 nm. For the sample G60 and S60, two clear peaks can be found from results, the first peak is located in the range of 10 nm–100 nm and the second peak around 1000 nm.

Fig. 10 (b) exhibits the pore size distribution curves of combining waste glass powder and GGBS with different proportions in mortars. The different recycled waste glass/GGBS ratio induces in the variation of the peak location and pore volume. The sample containing waste glass powder and GGBS with a proportion of 5:1 shows a higher and significant peak around 1000 nm compared with samples with waste glass/GGBS of 3:3 and 1:5.

When recycled waste glass powder and fly ash were used together, the change of the pore volume around 40 nm and another peak around 1000 nm can be found as shown in Fig. 14 (c). All samples show the similar shape of a peak around 40 nm, especially, F50G10 shows the highest peak here. After a higher waste glass powder proportion was conducted, this peak turns into weaker. These indicate that the increasing proportion of waste glass powder can reduce the pore volume around 40 nm. From the other side, the increase of waste glass powder amount enhances the pore volume from 100 nm to 1000 nm.

3.3.2. SEM

Fig. 11 presents the microstructure of different mortars. The left side is related to the pastes, while the right side is related to polished mortar samples. The improvement of the microstructure of pozzolanic materials blended concrete has been addressed in may studies (Li and Zhao, 2003a; Shayan and Xu, 2006; Zong et al., 2014). As shown in Fig. 11 (a), a dense structure is observed in the sample G60. The small amount of cubes in the red circle are corresponded to the residual calcium hydroxide (Li and Zhao,

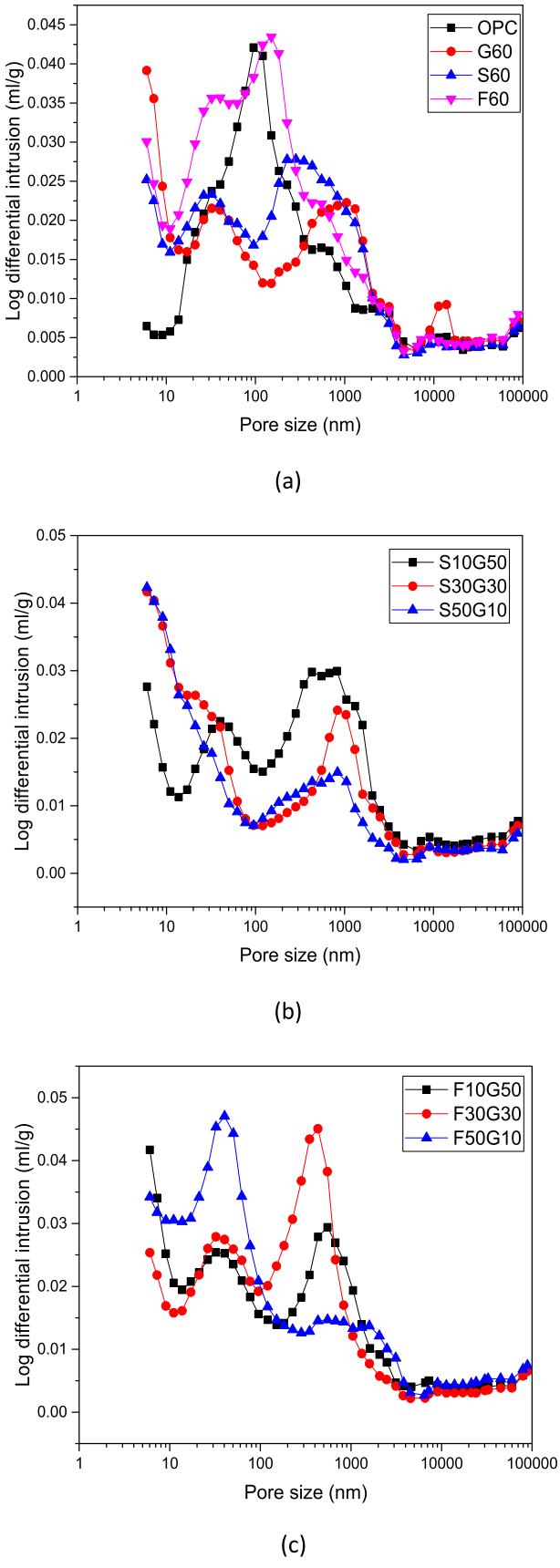

Fig. 10. Pore size distribution of different samples (a) OPC and binary samples (b) OPC-GGBS-waste glass samples (c) OPC-fly ash-waste glass samples.

2003b). In the case of high volume addition of waste glass powder, there are micro crack and an aggregation of unreacted glass particles, which are located between sand particles. This may relate to the higher porosity around 1000 nm. In addition, a thick ITZ is presented between the aggregate and the matrix, and a dense ITZ can also be found in high volume of GGBS sample as shown in Fig. 11 (b). In Fig. 11 (c), the unreacted fly ash sphere is covered by the loosely packed matrix, and a number of large calcium hydroxide crystals can be clearly identified. Compared to the other samples, the high volume fly ash sample presents a porosity structure of polished mortar sample. The larger calcium hydroxide crystal size and porous microstructure of high volume fly ash sample are responsible for the high D_{RCM}. This increase in calcium hydroxide crystal size in fly ash blended cement was also observed in Hu's study (Hu, 2014). When the recycled waste glass powder is incorporated with GGBS or fly ash, a denser microstructure is clearly exhibited as shown in Fig. 11 (d) and (e). In addition, a better compacting ITZ indicates that an improvement of microstructure occurred after the incorporation of recycled waste glass powder.

3.4. Rapid chloride migration

The results of rapid chloride migration of different mortars (aged 91 days) are shown in Fig. 12. The plain OPC mortar shows the highest D_{RCM} among all samples. For binary binder samples, after cement was replaced by the high volume of recycled waste glass, GGBS or fly ash, these samples (G60, S60 and F60) all show a lower D_{RCM} compared to the OPC. Especially for the G60 and S60, the D_{RCM} are reduced dramatically by 95% and 83.5%, respectively. At the same time, the D_{RCM} of the specimen incorporating high volume of fly ash (F60) only shows a reduction of 18.1% compared to the OPC. The incorporation of 60% recycled waste glass provides an excellent resistance to chloride migration compared to the GGBS and fly ash samples. In ternary binders, combining use recycled waste glass with GGBS or fly ash also exhibit better performance than only using GGBS or fly ash. In addition, it is interesting to notice that when the recycled waste glass is combined with fly ash in binders, the D_{RCM} presents a significant reduction with the increased amount of recycled waste glass.

The relationship between recycled waste glass content and rapid chloride migration coefficient in two different ternary binder is illustrated in Fig. 13. With the increase of the recycled waste glass amount in binders, cement-fly ash-recycled waste glass mixtures exhibit a drastic drop of D_{RCM}. At the same time, the reduction of D_{RCM} for OPC-GGBS-recycled waste glass mortars with increasing glass powder content is limited. This indicates that the incorporation of waste glass powder in fly ash blended mixtures present a more significant improvement of resistance to chloride migration than in GGBS blended mixtures. The improvement of the resistance to chloride migration by pozzolanic materials incorporation, for example GGBS or fly ash, were also identified by other studies (Kim et al., 2018; Leng et al., 2000b; Shi, 2004a). Generally, the interfacial transition zone (ITZ) of OPC concrete is rich in calcium hydroxide, which is the weak area in concrete for ion transportation. The addition of pozzolanic material consumes CH and then provides a dense ITZ, which is beneficial for the concrete. This is also confirmed in Section 3.4.2. Furthermore, the RCM test is based on the electric conductivity method, which can be affected by the conductivity of the concrete pore solution. Meanwhile, the ion dosage in the pore solution depends on the chemical composition of different binder systems. For example, in concrete containing pozzolanic materials, the change of chemical composition can be induced by the consumption of calcium hydroxide during (Jain and Neithalath, 2010a). As shown in Fig. 8, the increase of waste glass powder proportion in blended binders results in a decrease of

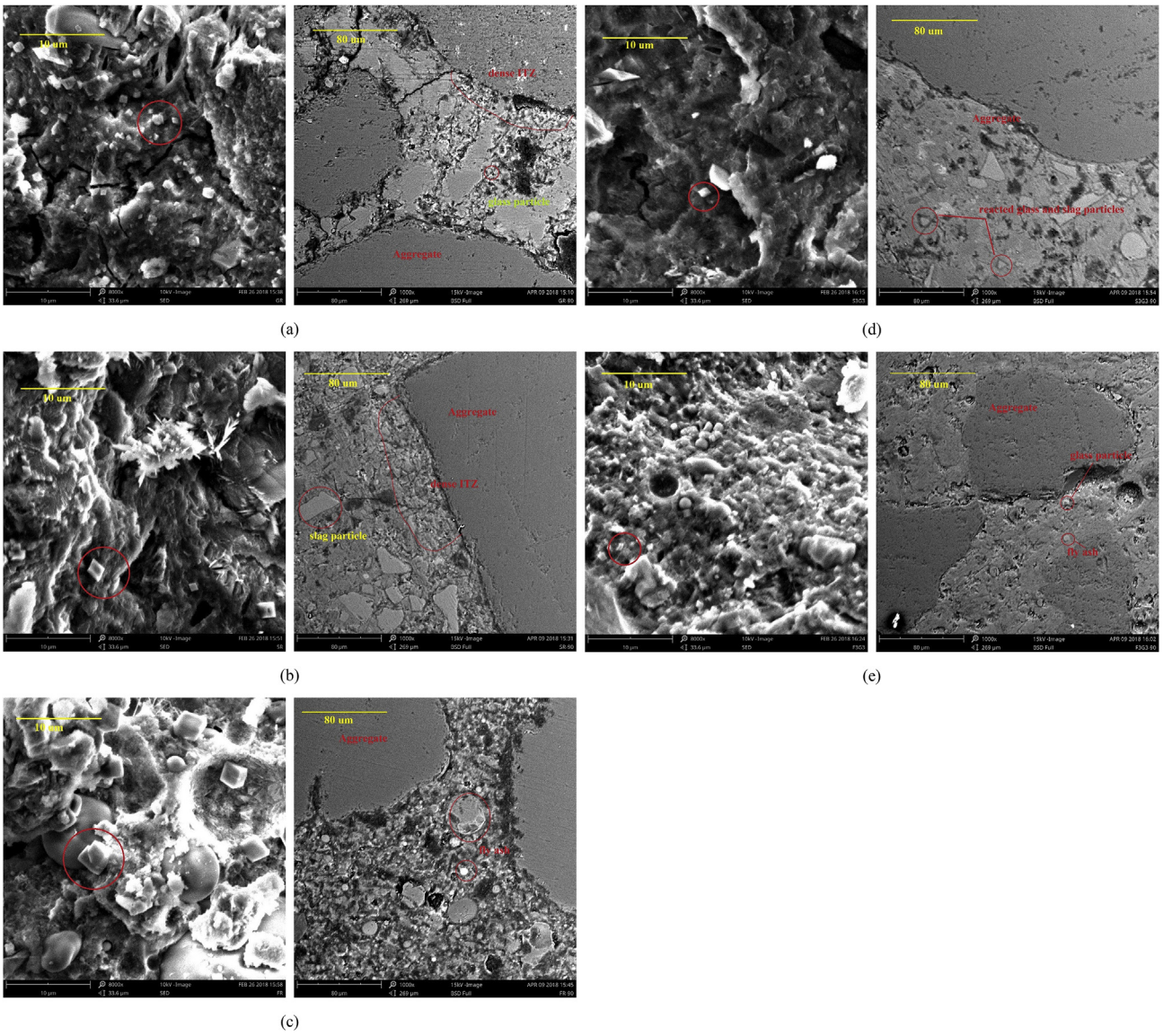

Fig. 11. SEM images of (a) G60, (b) S60, (c) F60, (d) S30G30 and (e) F30G30 (as shown in Table 1).

calcium hydroxide content after 91 days, which agrees with the reduction of D_{RCM}.

However, when comparing CH contents in GGBS ternary binders and fly ash ternary binders, it can be observed that although the GGBS ternary binders exhibit a higher CH content, it still presents a lower D_{RCM} compared to fly ash ternary binders. High volume fly ash sample (F60) shows a lower CH content compared to the high volume slag sample (S60), but a significantly higher D_{RCM}. This may be induced by the different microstructure of mixtures, for example, pore size structures, which will be discussed in the following.

The difference of pore size distributions can result in the observed variation in the chloride migration. It has been identified that using SCMs in concrete cause changes in concrete pore structure, which result in different resistance to chloride penetration (Liu et al., 2017; Shi, 2004b; Zong et al., 2014). The present research shows that the pore between 10 and 100 nm is mostly related to the coefficient of rapid chloride migration. The relationship between the volume of the capillary pores and the transport property of concrete has been addressed in many studies (Yu et al., 2017; Yu and Ye, 2013). For example, in Wu's study about microstructure and ITZ of blended cement, a reduction of chloride transport correlated with the decrease of volume between 10 and 100 nm (Wu et al., 2016), which is also in agreement with the present data. As described in microstructure-property on pozzolan-containing concrete by Paiva et al., the pozzolanic reaction occurred inside the capillary pores, as a consequence, a densification of micro pores was observed by the results of MIP (Paiva et al., 2017). This conclusion also supports the MIP results as previous discussion.

In this study, the G60 shows a great modified effect on mixtures microstructure. An obvious densification has been exhibited by MIP results. It is interesting to notice that the G60 show a similar pore size distribution as the S60. This indicates that the addition of 60% of waste glass particles has a potential to build similar microstructure as GGBS in concrete. On the contrary, although the 60% fly ash mortar exhibits a lower D_{RCM} than OPC, it displays an analogous pore size distribution curve as the OPC mortar. The reduction of D_{RCM} of high volume fly ash containing sample is mainly due to the decrease of electrical conductivity. The fly ash blended concrete can lower the alkalinity of the pore solution of concrete, which is

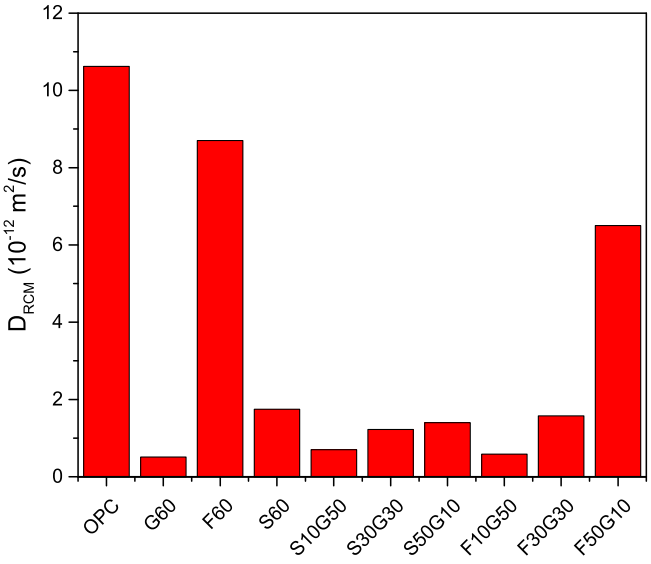

Fig. 12. Rapid chloride migration coefficient of mortars.

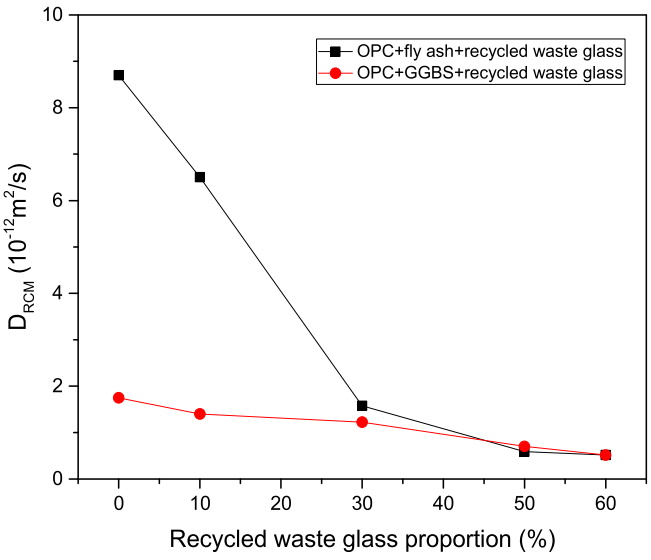

Fig. 13. The relationship between recycled waste glass content and rapid chloride migration coefficient.

related to the reduction of alkaline ions and hydroxyl ions (Shehata et al., 1999). In addition, the Friedel's salt in fly ash blended cement also corresponds to the enhancement of the resistance for chloride transportation (Jain and Neithalath, 2010b).

3.5. Mechanical performance

The compressive strength of mortars is shown in Table 4. High volume of glass powder, GGBS, and fly ash in binary binders result in different compressive at various ages. It is clear that the plain mortar (OPC) exhibits the higher compressive strength at early age and late age than the sample containing 60% glass powder, GGBS or fly ash. The best mechanical performance of mortar in binary binder system after 91 days curing is presented by G60, which is higher than the slag sample (S60) by 10.4% and the fly ash sample (F60) by 18%. However, the glass powder sample presents a poor mechanical performance at early ages, such as 7 days, compared to

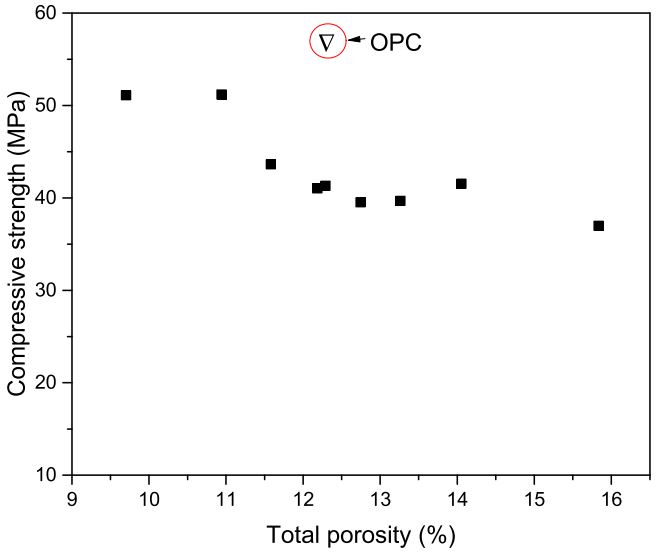

Fig. 14. The total porosity and compressive strength of blended samples.

other specimens. The compressive strength of G60 after 7 days curing shows a reduction of 47% and 26.4% compared to S60 and F60, respectively. However, the poor strength performance of G60 is improved significantly after had a long curing duration. For example, after 56 days, the strength of G60 is higher than that of S60 and F60.

In OPC-GGBS-recycled waste glass powder ternary samples, an obvious enhancement of strength at later ages can be observed compared to binary sample G60 and S60. Ternary samples S30G30 and S50G10 achieve the highest compressive strength after 91 days. At the early age, combining GGBS and glass powder improves early strength (7 days) gradually with the increasing of GGBS/glass powder ratio. The slag proportion contributes to the better performance at early age, which is due to the higher reactivity of GGBS.

The glass powder in OPC-fly ash-glass powder binder results in fewer effects on strength development. The increasing fly ash/glass powder ratio shows almost no influence on the early age strength but increases the strength after 28 days. Eventually, F50G10 achieves the highest compressive strength, which is higher than the fly ash binary sample (F60) by 12.3%.

In general, the high volume glass powder, slag and fly ash in ternary and binary binders result in lower strength compared to the plain OPC sample until 91 days. The low early strength can be found in all samples, especially for G60. After combining glass powder with GGBS or fly ash, the early strength can be improved, as well as the better performance at late age, for example, S50G10 and S30G30. The OPC-GGBS-glass powder binder exhibits significant better performance than the cement-fly ash-glass powder binder on compressive strength development. In many studies, the mechanical performance of blended concrete has been confirmed to correspond to the microstructure (Jeong et al., 2015; Lavergne et al., 2018; Yang et al., 2018). Fig. 14 exhibits the correlation between compressive strength and total porosity. It can be seen that the compressive strength performance of blended mortars depends on the variation of total porosity. A low porosity corresponds to the high compressive strength of blended mortars. From the section 3.3.1, S50G10 and S30G30 show a very low porosity compared to other samples, whereas exhibiting the highest compressive strength. A conclusion of combining application of small amounts of glass with GGBS can significantly enhance the mechanical performance of OPC-GGBS-recycled waste glass powder mortars can

Table 4
Strength performance of mortars.

Sample	Flexural strength (MPa)				Compressive strength (MPa)			
	7 days	28 days	56 days	91 days	7 days	28 days	56 days	91 days
OPC	6.74 ± 0.23	7.60 ± 0.19	8.39 ± 0.19	8.47 ± 0.43	41.91 ± 1.65	51.84 ± 0.84	55.25 ± 3.08	57.72 ± 1.60
F60	3.89 ± 0.12	5.07 ± 0.04	6.08 ± 0.20	6.26 ± 0.05	14.96 ± 0.56	22.47 ± 0.84	32.63 ± 2.09	36.99 ± 3.15
S60	5.07 ± 0.09	6.13 ± 0.11	6.16 ± 0.17	6.31 ± 0.25	20.79 ± 1.11	36.15 ± 1.09	38.15 ± 1.64	39.54 ± 0.56
G60	3.08 ± 0.08	5.12 ± 0.17	6.29 ± 0.14	6.69 ± 0.25	11.01 ± 0.49	29.08 ± 1.33	38.91 ± 1.77	43.65 ± 1.33
F10G50	3.86 ± 0.01	5.47 ± 0.12	5.95 ± 0.23	5.55 ± 0.03	13.66 ± 0.17	31.39 ± 0.54	33.78 ± 1.58	41.04 ± 0.63
F30G30	3.73 ± 0.11	5.64 ± 0.08	6.27 ± 0.17	6.26 ± 0.47	14.14 ± 0.47	32.60 ± 1.71	34.18 ± 0.95	39.68 ± 1.26
F50G10	3.80 ± 0.09	6.00 ± 0.02	7.25 ± 0.18	6.88 ± 0.04	14.66 ± 0.25	27.79 ± 1.20	37.91 ± 0.72	41.53 ± 1.57
S10G50	3.92 ± 0.17	5.54 ± 0.31	7.40 ± 0.33	7.63 ± 0.01	13.81 ± 0.59	33.64 ± 0.80	36.59 ± 1.70	41.30 ± 0.60
S30G30	4.23 ± 0.07	6.49 ± 0.02	8.19 ± 0.05	8.34 ± 0.22	17.27 ± 0.55	38.29 ± 0.60	49.85 ± 1.67	51.18 ± 1.42
S50G10	4.77 ± 0.13	6.83 ± 0.13	7.69 ± 0.09	7.95 ± 0.02	20.48 ± 0.60	39.43 ± 1.67	48.09 ± 3.72	51.11 ± 2.66

be addressed. However, the OPC sample shows a medium total porosity, while the highest compressive strength compared to blended mortars. This is induced by the unique pore size distribution, which is different from the blended samples as shown in Section 3.3.1.

4. Conclusions

This investigation evaluates mechanical and durability performance of mortars containing 60% SCMs (recycled waste glass powder, GGBS and fly ash) as binders. Different binary and ternary binders were conducted to study the compatibility of recycled waste glass powder with GGBS and fly ash. The fresh and hardened properties, reaction kinetics, resistance for rapid chloride migration, mechanical performance and pore structure were tested. The following conclusions can be formulated:

1. The isothermal calorimetry results indicate that combining recycled waste glass powder in GGBS or fly ash blended binders improve early reaction intensity and accelerate the hydration process.
2. 60% recycled glass binary binder presents the lowest calcium hydroxide after 91 days curing compared to 60% GGBS and 60% fly ash blended samples. The combination of recycled waste glass powder in GGBS or fly ash blended system results in a reduction of the residual calcium hydroxide amount and a denser microstructure of mortar samples.
3. Combining recycled waste glass powder with GGBS and fly ash provides a significantly better performance of resistance for rapid chloride migration compared to samples only blended with high volume GGBS or fly ash. A densification of capillary pores (10 nm−100 nm) is observed after blending recycled waste glass powder with GGBS or fly ash in binder system. Furthermore, a decrease of total pore volume can be induced by adding recycled waste glass powder in GGBS or fly ash blended mortars.
4. Combining recycled waste glass powder with GGBS or fly ash contributes to a better mechanical performance of mortars compared to samples containing waste glass powder only. The incorporation of 10% and 30% recycled waste glass powder in GGBS ternary binder can markedly decrease the total porosity of samples, which produces a comparable compressive strength of 51.11 MPa and 51.17 MPa, respectively, compared to 57.52 MPa of a plain OPC mortar.

Further studies will focus on the particle packing and hydration of ternary mixes including waste glass powder, and their effect on the performance of the concrete.

Acknowledgments

This research was supported by the funding of China Scholarship Council (No. 201606300062) and Eindhoven University of Technology.

References

Bijen, J., 1996. Benefits of slag and fly ash. Constr. Build. Mater. 10, 309–314.
Bouikni, A., Swamy, R.N., Bali, A., 2009. Durability properties of concrete containing 50% and 65% slag. Constr. Build. Mater. 23, 2836–2845.
Brouwers, H.J.H., 2016. Packing fraction of particles with a Weibull size distribution. Phys. Rev. E 94, 12905.
Chen, W., Brouwers, H.J.H., 2007. The hydration of slag, part 2: reaction models for blended cement. J. Mater. Sci. 42, 444–464.
Crossin, E., 2015. The greenhouse gas implications of using ground granulated blast furnace slag as a cement substitute. J. Clean. Prod. 95, 101–108.
Du, H., Tan, K.H., 2017. Properties of high volume glass powder concrete. Cement Concr. Compos. 75, 22–29.
Du, H., Tan, K.H., 2014. Waste glass powder as cement replacement in concrete. J. Adv. Concr. Technol. 12, 468–477.
Feiz, R., Ammenberg, J., Eklund, M., Helgstrand, A., Marshall, R., 2015. Improving the CO2 performance of cement, part I: utilizing life-cycle assessment and key performance indicators to assess development within the cement industry. J. Clean. Prod. 98, 272–281.
Garbev, K., Beuchle, G., Bornefeld, M., Black, L., Stemmermann, P., 2008a. Cell dimensions and composition of nanocrystalline calcium silicate hydrate solid solutions. Part 1: synchrotron-based x-ray diffraction. J. Am. Ceram. Soc. 91, 3005–3014.
Garbev, K., Bornefeld, M., Beuchle, G., Stemmermann, P., 2008b. Cell dimensions and composition of nanocrystalline calcium silicate hydrate solid solutions. Part 2: X-ray and thermogravimetry study. J. Am. Ceram. Soc. 91, 3015–3023.
Gholampour, A., Ozbakkaloglu, T., 2017. Performance of sustainable concretes containing very high volume Class-F fly ash and ground granulated blast furnace slag. J. Clean. Prod. 162, 1407–1417.
Häkkinen, T., 1993. The influence of slag content on the microstructure, permeability and mechanical properties of concrete Part 1 Microstructural studies and basic mechanical properties. Cement Concr. Res. 23, 407–421.
Hu, C., 2014. Microstructure and mechanical properties of fly ash blended cement pastes. Constr. Build. Mater. 73, 618–625.
Jain, J.A., Neithalath, N., 2010a. Chloride transport in fly ash and glass powder modified concretes – influence of test methods on microstructure. Cement Concr. Compos. 32, 148–156.
Jain, J.A., Neithalath, N., 2010b. Chloride transport in fly ash and glass powder modified concretes – influence of test methods on microstructure. Cement Concr. Compos. 32, 148–156.
Jeong, Y., Park, H., Jun, Y., Jeong, J.H., Oh, J.E., 2015. Microstructural verification of the strength performance of ternary blended cement systems with high volumes of fly ash and GGBFS. Constr. Build. Mater. 95, 96–107.
Jun-yuan, H., Scheetz, B.E., Roy, D.M., 1984. Hydration of fly ash-portland cements. Cement Concr. Res. 14, 505–512.
Kayali, O., Sharfuddin Ahmed, M., 2013. Assessment of high volume replacement fly ash concrete – concept of performance index. Constr. Build. Mater. 39, 71–76.
Keulen, A., Yu, Q.L., Zhang, S., Grünewald, S., 2018. Effect of admixture on the pore structure refinement and enhanced performance of alkali-activated fly ash-slag concrete. Constr. Build. Mater. 162, 27–36.
Kim, H.K., Lee, H.K., 2013. Effects of high volumes of fly ash , blast furnace slag , and bottom ash on flow characteristics , density , and compressive strength of high-strength mortar. J. Mater. Civ. Eng. 25, 662–665.
Kim, Y., Hanif, A., Usman, M., Munir, M.J., Kazmi, S.M.S., Kim, S., 2018. Slag waste incorporation in high early strength concrete as cement replacement: environmental impact and influence on hydration & durability attributes. J. Clean. Prod. 172, 3056–3065.

Kumar, A., Walder, B.J., Kunhi Mohamed, A., Hofstetter, A., Srinivasan, B., Rossini, A.J., Scrivener, K., Emsley, L., Bowen, P., 2017. The atomic-level structure of cementitious calcium silicate hydrate. J. Phys. Chem. C 121, 17188–17196.
Kurda, R., Silvestre, J.D., de Brito, J., Ahmed, H., 2018. Optimizing recycled concrete containing high volume of fly ash in terms of the embodied energy and chloride ion resistance. J. Clean. Prod. 194, 735–750.
Lavergne, F., Ben Fraj, A., Bayane, I., Barthélémy, J.F., 2018. Estimating the mechanical properties of hydrating blended cementitious materials: an investigation based on micromechanics. Cement Concr. Res. 104, 37–60.
Lee, H., Hanif, A., Usman, M., Sim, J., Oh, H., 2018. Performance evaluation of concrete incorporating glass powder and glass sludge wastes as supplementary cementing material. J. Clean. Prod. 170, 683–693.
Leng, F., Feng, N., Lu, X., 2000a. An experimental study on the properties of resistance to diffusion of chloride ions of fly ash and blast furnace slag concrete. Cement Concr. Res. 30, 989–992.
Leng, F., Feng, N., Lu, X., 2000b. Experimental study on the properties of resistance to diffusion of chloride ions of fly ash and blast furnace slag concrete. Cement Concr. Res. 30, 989–992.
Li, G., Zhao, X., 2003a. Properties of concrete incorporating fly ash and ground granulated blast-furnace slag. Cement Concr. Compos. 25, 293–299.
Li, G., Zhao, X., 2003b. Properties of concrete incorporating fly ash and ground granulated blast-furnace slag. Cement Concr. Compos. 25, 293–299.
Li, K., Zeng, Q., Luo, M., Pang, X., 2014. Effect of self-desiccation on the pore structure of paste and mortar incorporating 70% GGBS. Constr. Build. Mater. 51, 329–337.
Li, Y., Bao, J., Guo, Y., 2010. The relationship between autogenous shrinkage and pore structure of cement paste with mineral admixtures. Constr. Build. Mater. 24, 1855–1860.
Liu, G., Florea, M.V.A., Brouwers, H.J.H., 2019. Performance evaluation of sustainable high strength mortars incorporating high volume waste glass as binder. Constr. Build. Mater. 202, 574–588.
Liu, G., Florea, M.V.A., Brouwers, H.J.H., 2018. The Hydration and Microstructure Characteristics of Cement Pastes with High Volume Organic-Contaminated Waste Glass Powder.
Liu, J., Wang, X., Qiu, Q., Ou, G., Xing, F., 2017. Understanding the effect of curing age on the chloride resistance of fly ash blended concrete by rapid chloride migration test. Mater. Chem. Phys. 196, 315–323.
Mo, K.H., Johnson Alengaram, U., Jumaat, M.Z., Yap, S.P., 2015. Feasibility study of high volume slag as cement replacement for sustainable structural lightweight oil palm shell concrete. J. Clean. Prod. 91, 297–304.
Moon, H.Y., Kim, H.S., Choi, D.S., 2006. Relationship between average pore diameter and chloride diffusivity in various concretes. Constr. Build. Mater. 20, 725–732.
Mostafa, N.Y., Brown, P.W., 2005. Heat of hydration of high reactive pozzolans in blended cements: isothermal conduction calorimetry. Thermochim. Acta 435, 162–167.
Nocuò-Wczelik, W., 1999. Effect of Na and Al on the phase composition and morphology of autoclaved calcium silicate hydrates. Cement Concr. Res. 29, 1759–1767.
Ogawa, K., Uchikawa, H., Takemoto, K., Yasui, I., 1980. The mechanism of the hydration in the system C3S-pozzolana. Cement Concr. Res. 10, 683–696.
Oh, J.E., Monteiro, P.J.M., Jun, S.S., Choi, S., Clark, S.M., 2010. The evolution of strength and crystalline phases for alkali-activated ground blast furnace slag and fly ash-based geopolymers. Cement Concr. Res. 40, 189–196.
Paiva, H., Silva, A.S., Velosa, A., Cachim, P., Ferreira, V.M., 2017. Microstructure and hardened state properties on pozzolan-containing concrete. Constr. Build. Mater. 140, 374–384.
Plowman, C., Cabrera, J.G., 1984. Mechanism and kinetics of hydration of C3A and C4AF. Extracted from cement. Cement Concr. Res. 14, 238–248.
Puertas, F., Fernández-Jiménez, A., 2003. Mineralogical and microstructural characterisation of alkali-activated fly ash/slag pastes. Cement Concr. Compos. 25, 287–292.
Ramakrishnan, K., Pugazhmani, G., Sripragadeesh, R., Muthu, D., Venkatasubramanian, C., 2017. Experimental study on the mechanical and durability properties of concrete with waste glass powder and ground granulated blast furnace slag as supplementary cementitious materials. Constr. Build. Mater. 156, 739–749.
Ranjbar, N., Behnia, A., Alsubari, B., Moradi Birgani, P., Jumaat, M.Z., 2016. Durability and mechanical properties of self-compacting concrete incorporating palm oil fuel ash. J. Clean. Prod. 112, 723–730.
Rashad, A.M., 2015. An investigation of high-volume fly ash concrete blended with slag subjected to elevated temperatures. J. Clean. Prod. 93, 47–55.
Schwarz, N., Neithalath, N., 2008. Influence of a fine glass powder on cement hydration: comparison to fly ash and modeling the degree of hydration. Cement Concr. Res. 38, 429–436.
Shao, Y., Lefort, T., Moras, S., Rodriguez, D., 2000. Studies on concrete containing ground waste glass. Cement Concr. Res. 30, 91–100.
Shayan, A., Xu, A., 2006. Performance of glass powder as a pozzolanic material in concrete: a field trial on concrete slabs. Cement Concr. Res. 36, 457–468.
Shehata, M.H., Thomas, M.D.A., Bleszynski, R.F., 1999. The effects of fly ash composition on the chemistry of pore solution in hydrated cement pastes. Cement Concr. Res. 29, 1915–1920.
Shi, C., 2004a. Effect of mixing proportions of concrete on its electrical conductivity and the rapid chloride permeability test (ASTM C1202 or ASSHTO T277) results. Cement Concr. Res. 34, 537–545.
Shi, C., 2004b. Effect of mixing proportions of concrete on its electrical conductivity and the rapid chloride permeability test (ASTM C1202 or ASSHTO T277) results. Cement Concr. Res. 34, 537–545.
Shi, C., Wu, Y., Riefler, C., Wang, H., 2005. Characteristics and pozzolanic reactivity of glass powders. Cement Concr. Res. 35, 987–993.
Siad, H., Lachemi, M., Sahmaran, M., Mesbah, H.A., Hossain, K.M.A., 2018. Use of recycled glass powder to improve the performance properties of high volume fly ash-engineered cementitious composites. Constr. Build. Mater. 163, 53–62.
Song, S., Jennings, H.M., 1999. Pore solution chemistry of alkali-activated ground granulated blast-furnace slag. Cement Concr. Res. 29, 159–170.
Spiesz, P., Brouwers, H.J.H., 2012. Influence of the applied voltage on the rapid chloride migration (RCM) test. Cement Concr. Res. 42, 1072–1082.
Torres-Carrasco, M., Puertas, F., 2015. Waste glass in the geopolymer preparation. Mechanical and microstructural characterisation. J. Clean. Prod. 90, 397–408.
Van Tuan, N., Ye, G., van Breugel, K., Fraaij, A.L.A., Bui, D.D., 2011. The study of using rice husk ash to produce ultra high performance concrete. Constr. Build. Mater. 25, 2030–2035.
Wan, S., Zhou, X., Zhou, M., Han, Y., Chen, Y., Geng, J., Wang, T., Xu, S., Qiu, Z., Hou, H., 2018. Hydration characteristics and modeling of ternary system of municipal solid wastes incineration fly ash-blast furnace slag-cement. Constr. Build. Mater. 180, 154–166.
Wongkeo, W., Thongsanitgarn, P., Ngamjarurojana, A., Chaipanich, A., 2014. Compressive strength and chloride resistance of self-compacting concrete containing high level fly ash and silica fume. Mater. Des. 64, 261–269.
Wu, K., Shi, H., Xu, L., Ye, G., De Schutter, G., 2016. Microstructural characterization of ITZ in blended cement concretes and its relation to transport properties. Cement Concr. Res. 79, 243–256.
Yang, J., Su, Y., He, X., Tan, H., Jiang, Y., Zeng, L., Strnadel, B., 2018. Pore structure evaluation of cementing composites blended with coal by-products: calcined coal gangue and coal fly ash. Fuel Process. Technol. 181, 75–90.
Yang, K.-H., Jung, Y.-B., Cho, M.-S., Tae, S.-H., 2015. Effect of supplementary cementitious materials on reduction of CO2 emissions from concrete. J. Clean. Prod. 103, 774–783.
Yazıcı, H., 2007. The effect of curing conditions on compressive strength of ultra high strength concrete with high volume mineral admixtures. Build. Environ. 42, 2083–2089.
Yu, Z., Ma, J., Ye, G., van Breugel, K., Shen, X., 2017. Effect of fly ash on the pore structure of cement paste under a curing period of 3 years. Constr. Build. Mater. 144, 493–501.
Yu, Z., Ye, G., 2013. The pore structure of cement paste blended with fly ash. Constr. Build. Mater. 45, 30–35.
Zeng, Q., Li, K., Fen-chong, T., Dangla, P., 2012. Pore structure characterization of cement pastes blended with high-volume fly-ash. Cement Concr. Res. 42, 194–204.
Zong, L., Fei, Z., Zhang, S., 2014. Permeability of recycled aggregate concrete containing fly ash and clay brick waste. J. Clean. Prod. 70, 175–182.
Zuquan, J., Wei, S., Yunsheng, Z., Jinyang, J., Jianzhong, L., 2007. Interaction between sulfate and chloride solution attack of concretes with and without fly ash. Cement Concr. Res. 37, 1223–1232.